44th AIAA Aerospace Sciences Meeting and Exhibit, 9–12 January 2006, Reno NV

Optimization of Nonlinear Error Sources for Weighted Essentially Non-Oscillatory Methods in Direct Numerical Simulations of Compressible Turbulence

Ellen M. Taylor,* Minwei Wu,* and M. Pino Martín†
Princeton University, Princeton NJ 08544

Weighted essentially non-oscillatory (WENO) methods have been developed to simultaneously provide robust shock-capturing in compressible fluid flow and avoid excessive damping of fine-scale flow features such as turbulence. Under certain conditions in compressible turbulence, however, numerical dissipation remains unacceptably high even after optimization of the linear component that dominates in smooth regions. We therefore construct and evaluate WENO schemes that also reduce dissipation due to two independent *non*linear error sources: (i) the smoothness measurement that governs the application of stencil adaption away from the linear optimal stencil, and (ii) the numerical accuracy (e.g. order-of-accuracy and bandwidth) properties of the less favorable stencils that take over when adaption engages. Direct numerical simulations (DNS) include one-dimensional test cases and three-dimensional compressible isotropic turbulence. Although efforts to address the second source listed above fail to meaningfully alter WENO performance, the smoothness measurement modification inspired by the first source both significantly enhances numerical accuracy and generates negligible additional computational expense. Moreover, this technique appears to be broadly effective regardless of flow configuration.

I. Introduction

The detailed simulation of compressible turbulence requires numerical methods that simultaneously avoid excessive damping of spatial features over a large range of length scales and prevent spurious oscillations near shocks and shocklets (small transient shocks) through robust shock-capturing. Numerical schemes that were developed to satisfy these constraints include, among others, weighted essentially non-oscillatory (WENO) methods.[1] WENO schemes compute numerical fluxes using several different candidate stencils and form a final flux approximation by summing weighted contributions from each stencil. Smoothness measurements cause stencils that span large flow field gradients to be assigned small relative weights so that a nearly discontinuous shock would provide a weight of almost zero to any stencil containing it. In smooth regions, the relative values of the weights are designed to be optimal by some gauge such as maximum order of accuracy or maximum bandwidth-resolving efficiency.

Jiang and Shu[2] cast the WENO methodology into finite-difference form and provide an efficient implementation of robust and high-order-accurate WENO schemes. Unfortunately, these schemes often generate excessive numerical dissipation for detailed simulations of turbulence, especially for large-eddy simulations (LES).[3] WENO dissipation arises from two distinct sources: (i) the optimal stencil, which on its own describes a linear scheme, and (ii) the adaption mechanism, which drives the final numerical stencil away from the optimal one. Bandwidth optimization can reduce the dissipation of the optimal stencil;[4,5] and Martín et al.[5] demonstrate that such a bandwidth-optimized WENO method indeed reduces numerical dissipation and provides accurate results for direct numerical simulations (DNS) of isotropic turbulence and turbulent boundary layers.

*Ph.D. Student and AIAA Member.
†Assistant Professor and AIAA Member.

Nonetheless, engaging the nonlinear WENO adaption mechanism still causes significant local dissipation that can negatively affect global flow properties. Though higher resolution compensates for this, in some cases adequately increasing the number of grid points is not feasible. According to Martín,[6] LES of turbulent boundary layers fail with these linearly optimized WENO schemes because of insufficient distinction between shock-containing and smooth regions on typical LES grids. Additionally, Wu et al.[7] encounter disparities between DNS and experiments of shock/turbulent-boundary-layer interactions and determine that nonlinear WENO dissipation is responsible for the disagreement even at the highest possible resolutions.

The purpose of this paper is to construct and evaluate linearly optimized WENO schemes that also reduce dissipation due to nonlinear error sources for DNS of compressible turbulence. We separately address two such sources: (i) the smoothness measurement that governs the application of WENO stencil adaption, and (ii) the coefficients of the individual candidate stencils that govern numerical accuracy when adaption engages. Section II describes the symmetric WENO methodology, bandwidth optimization procedures, and three-dimensional turbulent flow configurations in which we test the modified WENO schemes. In Sections III and IV, we present motivations for and derivations of techniques that aid in suppressing error from the two sources listed above. These techniques are (i) overwriting smoothness measurement values with limiting values under certain conditions and (ii) bandwidth-optimizing each candidate stencil in addition to the optimal one. Sections III and IV also include results from numerical simulations.

II. Background

A. Symmetric WENO Methodology

We describe the symmetric WENO methodology[4,5] in the context of the one-dimensional linear advection equation,

$$\frac{\partial u}{\partial t} + \frac{\partial}{\partial x} f(u) = 0 \tag{1}$$

This model equation represents the decoupled forms of equations belonging to any system of hyperbolic conservation laws after a transformation from physical into characteristic space. If the spatial domain is discretized such that $x_i = i\Delta$, in which Δ is the grid spacing, and $u_i = u\left(x_i\right)$, Eq. (1) may be cast into the semidiscretized form

$$\frac{du_i}{dt} = -\frac{1}{\Delta}\left(\hat{f}_{i+\frac{1}{2}} - \hat{f}_{i-\frac{1}{2}}\right) \tag{2}$$

in which $\hat{f}_{i+1/2}$ is a numerical approximation of $f\big(u(x_{i+1/2})\big)$. Once the right-hand side of this expression has been evaluated, numerical techniques for solving ordinary differential equations, such as Runge-Kutta methods, may be employed to advance the solution in time. In order to ensure stability, procedures that approximate $f(u)$ split it into $f^+(u)$, which has a strictly non-negative derivative, and $f^-(u)$, which has a strictly non-positive one.

WENO schemes compute $\hat{f}^+_{i+1/2}$ through interpolating polynomials on a number of candidate stencils each containing r grid points. In the symmetric WENO method, there are $(r+1)$ stencils in total. The one fully upwinded stencil ranges from $(i-r+1)$ to i, the one fully downwinded stencil ranges from $(i+1)$ to $(i+r)$, and the other stencils fall in between these two extremes. Figure 1 provides a schematic of this arrangement. Throughout this paper, we will abbreviate any WENO implementation in which the candidate stencils contain r points as "WENO-r."

If the flux approximation on stencil k, which contains r grid points, is designated q^r_k and the weight assigned to that stencil is ω_k, the final numerical approximation becomes

$$\hat{f}^+_{i+\frac{1}{2}} = \sum_{k=0}^{r} \omega_k q^r_k \tag{3}$$

Specifically, q^r_k emerge from polynomial interpolants of maximal order r and are defined as

$$q^r_k \Big|_{i+\frac{1}{2}} = \sum_{l=0}^{r-1} a^r_{kl}\, f(u_{i-r+k+l+1}) \tag{4}$$

in which a_{kl}^r are tabulated coefficients; and ω_k are normalized forms of weights α_k defined as

$$\alpha_k = \frac{C_k^r}{(\varepsilon + IS_k)^p} \tag{5}$$

in which ε prevents division by zero, IS_k is a smoothness measurement that becomes large when discontinuities are present within stencil k, and p may be varied to increase or decrease WENO adaption sensitivity. $p = 1$ typically provides sufficient adaption with minimal dissipation. In completely smooth regions, each stencil is equally desirable, and ω_k revert to the optimal weights C_k. As formulated by Jiang and Shu,[2]

$$IS_k = \sum_{m=1}^{r-1} \Delta^{2m-1} \int_{x_{i-1/2}}^{x_{i+1/2}} \left[\frac{\partial^m}{\partial x^m} q_k^r(x) \right]^2 dx \tag{6}$$

in which $q_k^r(x)$ is an interpolating polynomial for the flux that may or may not be the same as the one that leads to $q_k^r\big|_{i+1/2}$ in Eq. (4). Equivalently,

$$IS_k = \sum_{l=0}^{r-1} \sum_{m=0}^{r-1} d_{klm}^r \, f(u_{i-r+k+l+1}) \, f(u_{i-r+k+m+1}) \tag{7}$$

in which d_{kml}^r are the coefficients that arise from Eq. (6).

The corresponding stencil diagram for $\hat{f}_{i+1/2}^-$ is simply a mirror image of Fig. 1. Because the total number of data points available to the symmetric WENO algorithm is $2r$, its maximum order of accuracy is also $2r$. In practice, the weight of the fully downwinded stencil ω_r is artificially constrained to be no greater than the least of the others so that adverse stability effects are avoided. Throughout this paper, we will abbreviate a WENO implementation in which the *candidate* stencils contain r points and the *optimal* stencil is formally nth-order accurate as "WENO-r/n." $n < 2r$ implies that bandwidth optimization has been applied to the optimal stencil, and $n < r$ implies that bandwidth optimization has been applied to both the optimal and candidate stencils.

The continuity of the WENO weighting process allows the performance characteristics of the final numerical stencil to fall anywhere between those of the least favorable candidate stencil and those of the optimal stencil. In order to gauge this variation quantitatively but efficiently in a flow field, Weirs[4] proposed a combination of the adaptive stencil weights called the nonlinearity index (NI). It is essentially a measure of the degree of departure from the optimal stencil and is defined as

$$NI = \left(\sum_{k=0}^{r} \left[1 - \frac{(r+1)\,(\alpha_k / C_k)}{\sum_{l=0}^{r} (\alpha_l / C_l)} \right]^2 \right)^{\frac{1}{2}} \tag{8}$$

This definition forces NI to always be non-negative, and only the optimal stencil can provide a value of zero. It reaches its theoretical maximum, which is $\sqrt{r\,(r+1)}$, when any one candidate stencil is chosen exclusively. Ideally, in smooth regions where WENO adaption is unnecessary, NI should remain much less than this maximum so that the favorable performance capabilities of the optimal stencil are realized.

B. Bandwidth Optimization

Bandwidth-resolving efficiency quantifies the ability of a numerical approximation to resolve a range of spatial frequencies and is therefore important for the detailed simulation of turbulence, in which relevant length scales span several orders of magnitude. The computational grid serves as the framework for bandwidth properties: the largest resolvable wavelength is equal to the length of the domain, and the smallest is equal to two grid spacings. The latter, however, is a theoretical limit because numerical methods may impose additional constraints. Though spectral methods can fully resolve all available wavenumbers, their global operations render them inefficient for parallel computing. Alternatively, finite-difference schemes, which are local in nature and thus minimize interprocessor communication, always limit bandwidth-resolving efficiency. WENO methods belong to the second class.

The bandwidth properties of linear numerical schemes are determined by Fourier analysis. Consider a pure harmonic function

$$f(x) = e^{ikx} \tag{9}$$

in which x is position and k is wavenumber. Then

$$f'(x) = ik\, f(x) \tag{10}$$

and, if we define n as any integer and Δ as grid spacing,

$$f(x + n\Delta) = e^{ink\Delta}\, f(x) \tag{11}$$

A general finite-difference method approximates the first derivative according to the formula

$$f'(x) = \frac{1}{\Delta} \sum_n c_n\, f(x + n\Delta) \tag{12}$$

in which c_n are nondimensional coefficients unique to a particular scheme. We may equate Eqs. (10) and (12) to yield

$$ik'\, f(x) = \frac{1}{\Delta} \sum_n c_n\, e^{ink\Delta}\, f(x) \tag{13}$$

If we designate $\kappa = k\Delta$, this reduces to

$$\kappa'(\kappa) = -i \sum_n c_n\, e^{in\kappa} \tag{14}$$

κ' is known as the modified wavenumber, and a numerical method that fully resolved all wavenumbers would produce $\kappa' = \kappa$ for $0 \leq \kappa \leq \pi$. $\Re(\kappa')$ describes phase characteristics and $\Im(\kappa')$ describes amplitude characteristics.

The primary approach to optimizing bandwidth properties is to delay the separation of $\Re(\kappa')$ from $\kappa' = \kappa$ to the highest feasible wavenumber. For such a process Lele[8] defines phase error as $[\Re(\kappa') - \kappa]/\kappa$ and bandwidth-resolving efficiency index as the value of κ/π for which this error first rises above an arbitrary threshold ε. A secondary and often interwoven approach to optimizing bandwidth properties is to shift amplitude errors to those wavenumbers for which the phase errors are already considerable. This allows small amounts of deliberate dissipation to continue to stabilize a simulation without corrupting otherwise pristine data. Balanced contributions from both approaches can be achieved by minimizing an integrated error function originally due to Lockard et al.[9] and later modified by Weirs:[4]

$$I = \int_0^\pi e^{\nu(\pi-\kappa)} \left(\sigma \left[\Re(\kappa' - \kappa) \right]^2 + (1-\sigma) \left[\Im(\kappa') - \gamma \sin^\mu \left(\tfrac{1}{2}\kappa \right) \right]^2 \right) d\kappa \tag{15}$$

Increasing σ places more emphasis on reducing phase errors rather than amplitude errors; increasing ν places more emphasis on reducing errors at lower wavenumbers; and adjusting γ and μ alters the incentive for neutrally stable schemes to favor dissipative amplitude errors over dispersive errors.

If the WENO adaption mechanism is switched entirely off, the optimal stencil weights form a linear numerical scheme to which Fourier analysis can be applied. Figure 2 presents $\kappa'(\kappa)$ for the bandwidth-optimized optimal stencils of various symmetric WENO schemes and, for reference, several well-established central Padé schemes.[8] Above $\kappa' = 0$ is $\Re(\kappa')$, and below is $\Im(\kappa')$, which in this case is uniformly dissipative.

C. DNS of Isotropic Turbulence

Because it is difficult to artificially mimic the sensitivity of turbulent features to numerical dissipation with simpler configurations, we include among our test cases three-dimensional direct numerical simulations (DNS) of decaying isotropic turbulence. Isotropic turbulence is a canonical flow field that realistically represents the small scales of many turbulent flows. The physical domain is a three-dimensional cube with periodic boundary conditions and an edge length such that the large-scale turbulence statistics are sufficiently uncorrelated between the center and edges. An evenly-spaced Cartesian grid discretizes this domain into N^3 points. We approximate the viscous terms of the Navier-Stokes equations with fourth-order-accurate finite differences and advance the solution in time with a third-order-accurate Runge-Kutta scheme.

The following two parameters are important for the generation of an initial field: the turbulent Mach number

$$M_t = \frac{q}{\langle a \rangle} \tag{16}$$

in which $\langle a \rangle$ is the average speed of sound and q is the root-mean-squared velocity summed over all directions, and the Reynolds number based on the Taylor microscale

$$Re_\lambda = \frac{\langle \rho \rangle \, u'_{\text{rms}} \lambda}{\langle \mu \rangle} \tag{17}$$

in which u'_{rms} is the root-mean-squared velocity and λ is the Taylor microscale. Note that M_t and Re_λ are not constant throughout a simulation because the global strength of turbulent fluctuations steadily decays over time without external forcing, which we do not include.

III. Relative Smoothness Limiter

Because the optimal stencil of a WENO scheme provides optimal performance in smooth regions, any technique that discourages unnecessary adaption can improve WENO dissipation characteristics in compressible turbulence. The following approach requires modification of the smoothness measurement and does *not* affect the candidate stencil coefficients a_{kl} in Eq. (4) or optimal stencil weights.

A. Theory

When the polynomial interpolant $q_k^r(x)$ in Eq. (6) is order-optimized (i.e. replicates tabulated data exactly), the Taylor expansion of IS_k yields

$$IS_k = \Delta^2 \left[f'(u_i) \right]^2 + O\left(\Delta^4\right) \tag{18}$$

Ideally, in smooth regions where WENO adaption is unnecessary, IS_k should be of the order of ε from Eq. (5); in other words, $IS_k \ll 1$. Now consider a linearly advected smooth sinusoidal function of nondimensional wavenumber κ (nondimensionalized by Δ):

$$f(u(x)) = u(x) = \sin\left(\frac{\kappa x}{\Delta}\right) \tag{19}$$

In this case, Eq. (18) becomes

$$IS_k(x) = \kappa^2 \cos^2\left(\frac{\kappa x}{\Delta}\right) + O\left(\Delta^4\right) \tag{20}$$

Thus for smoothly varying fuctions, $IS_k < 1$ requires $\kappa < 1$, which corresponds to a grid resolution of more than roughly six grid points per wavelength (PPW). To ensure that $IS_k < 0.1$ more than twenty points per wavelength are necessary. These restrictions indicate that the WENO smoothness measurement as defined in Eq. (6) triggers adaption too readily and thereby causes unnecessarily degradation of WENO performance.

Jiang and Shu[2] suggest that the over-adaption tendencies of WENO methods may be mitigated by redefining the smoothness measurement IS_k at points where it falls below a threshold value.

$$IS_k = \begin{cases} 0, & IS_k < \alpha \\ IS_k, & \text{otherwise} \end{cases} \tag{21}$$

In this procedure, effectual values of the absolute limiter α are arbitrary and strongly depend on the specific flow field configuration. Because it is preferable to achieve wide applicability to general turbulent flows, we propose a modified limiting procedure:

$$IS_k = \begin{cases} 0, & R(IS) < \alpha \\ IS_k, & \text{otherwise} \end{cases} \tag{22}$$

in which

$$R(IS) = \frac{\max\limits_{0 \le k \le r} IS_k}{\varepsilon + \min\limits_{0 \le k \le r} IS_k} \tag{23}$$

and in turn ε is the value employed in Eq. (5). Though the relative limiter α is still arbitrary, the focus on relative rather than absolute thresholds allows a general effectual value to be derived. Figure 3 displays the WENO-3 $R(IS)$ for the sinusoidal wave described above on grids providing six, eight, and twelve points per wavelength. It is apparent that for six or more points per wavelength, $R(IS)$ is less than one order of magnitude, and therefore we set $\alpha = 10$ in Eq. (22). Any WENO method that employs the relative limiting procedure with this threshold value will be referred to as WENO-RL.

B. Numerical Simulations

The Shu-Osher problem is an ideal one-dimensional flow configuration for testing numerical methods that must simultaneously capture shocks and avoid damping turbulent structures. Its initial conditions consist of a perfect normal shock with imposed density fluctuations downstream, and as time progresses, these fluctuations interact with and become altered by the shockwave. In Fig. 4(a), we present WENO-3/3 and WENO-3/3-RL nonlinearity index profiles for Shu-Osher simulations on a 200-point grid. They indicate that in the physically correct high-frequency region immediately upstream of the main shock, the WENO-3/3-RL scheme, unlike the WENO-3/3 scheme, does not adapt at all and thus employs its optimal stencil. Everywhere else, including among the upstream low-frequency fluctuations, the adaption mechanisms of both schemes perform similarly. Because the high-frequency oscillations are smooth and the left edges of the low-frequency fluctuations are shocklets, this WENO-3/3-RL behavior is exactly what the relative limiting procedure was designed to achieve. The WENO-3/3 and WENO-3/3-RL density profiles of Fig. 4(b) confirm that the result is elimination of excessive dissipation without endangerment of the shock-capturing capability.

We next investigate the effectiveness of the relative limiter in simulations of three-dimensional compressible isotropic turbulence. Figure 5 shows the temporal evolution of turbulent kinetic energy for $N = 80$ and initial $Re_\lambda = 35$ and $M_t = 0.7$ as computed by WENO-3/3, WENO-3/3-RL, WENO-4/4, and WENO-4/4-RL schemes. Grid-converged results for $N = 128$ are also included. Although neither WENO-3/3 method attains grid convergence with $N = 80$, the excess dissipation generated by the WENO-3/3-RL scheme is only about as much as that of the more computationally expensive WENO-4/4 scheme. In addition, the WENO-4/4-RL scheme, unlike the others, does indeed achieve grid convergence with merely $N = 80$ and is therefore the most computationally efficient.

IV. Candidate Stencil Bandwidth Optimization

WENO adaption is necessary in simulations of compressible flow; thus any technique that improves the performance characteristics of isolated WENO candidate stencils can also reduce excessive dissipation in turbulence. In this section, the smoothness measurement retains the unmodified form presented in Section II; in other words, no limiting procedures are employed.

A. Theory

Though the selection of any one candidate stencil to the exclusion of all others is rare, inspection of the bandwidth properties of individual candidates elucidates the lower limits of WENO performance. The bandwidth properties of the $k = 0$ and $k = 1$ order-optimized candidate stencils of the WENO-3 method are presented in Fig. 6 along with the properties of the optimal stencil of the WENO-3/3 scheme for reference. In addition, bandwidth-resolving efficiency indices for $\varepsilon = 1.1\%$ and $\varepsilon = 2.5\%$ are listed in Table 1 for all candidates. Whereas the optimal stencil adequately resolves roughly half of the available wavenumber spectrum, isolated candidate stencils are capable only of resolving less than a third, and the $k = 0$ (outside) stencil fares especially poorly. Though the excessive phase error of the $k = 1$ (inside) stencil is not as severe, its dissipation characteristics are not significantly more favorable than those of the $k = 0$ stencil.

We find that for WENO-3 and WENO-4 methods, bandwidth optimization of the candidate stencils fails to meaningfully improve bandwidth properties until their order of accuracy has been reduced to first order. Ponziani et al.[10] investigate such bandwidth-optimized stencils and observe modest gains in both theory and numerical simulations; however, they note that such a large reduction in order of accuracy interferes with the benefits of grid refinement in detailed simulations of turbulence. We therefore restrict our attention to bandwidth-optimized candidate stencils that retain at least second-order accuracy.

For WENO-5 methods, which allow for fifth-order-accurate candidate stencils, nontrivial improvement of bandwidth properties emerges for optimization procedures that preserve orders of accuracy as high as three.

If n is the order of accuracy of the candidates, the order of accuracy of the optimal stencil must lie between n and $(r+n)$. We choose nth-order accuracy in order to maintain the same number of free parameters for bandwidth-optimization of the optimal stencil as are available in the original WENO-5/5 scheme. After considering various values of ν and σ in Eq. (15) for $n=3$, we determine that $\nu=8$ and $\sigma=\frac{1}{2}$ produce the most desirable bandwidth improvement, except for the $k=0$ and $k=5$ (outside) stencils, for which $\sigma=\frac{3}{4}$ is best. To maintain consistency with the ideal parameters for optimizing the optimal stencil,[4,5] we keep nonzero γ and μ; but the original amplitude errors of the candidate stencils are sufficiently far from neutral that the impact of these two factors is negligible.

Figure 7 shows the bandwidth properties of the $k=0$, $k=1$, and $k=2$ candidate stencils of both the original WENO-5/5 scheme and the new WENO-5/3 scheme as well as the properties of the WENO-5/5 optimal stencil for reference. In addition, Tables 2 and 3 list the bandwidth-resolving efficiency indices and improvement percentages for $\varepsilon=1.0\%$ and $\varepsilon=2.5\%$, respectively. Meaningful reduction of both phase and amplitude errors is evident for all candidates, even for the $k=2$ and $k=3$ (inside) stencils. Though the resolving efficiency indices of the $k=0$ and $k=5$ stencils decrease for $\varepsilon=1.0\%$, the twofold increases for $\varepsilon=2.5\%$ justify this trade-off. For the higher error tolerance, the phase properties of the WENO-5/3 candidate stencils compare favorably with those of a fourth-order central Padé scheme,[8] which produces a resolving efficiency index of 0.438.

B. Numerical Simulations

We first focus on the ability of the WENO-5/3 scheme to faithfully capture discontinuities without spurious oscillations by simulating a one-dimensional inviscid shock tube on a 256-point grid. The density profile across the resulting contact discontinuity is displayed in Fig. 8 for the WENO-3/3, WENO-4/4, WENO-5/5, and WENO-5/3 schemes. These schemes produce identical results for the remaining shock tube features, including the compression shock, so we do not show those profiles. We have set $p=1.0$ as the default working value in Eq. (5) and observe in Fig. 8 that this value fails to induce sufficient adaption for both WENO-5 methods. Incrementally raising p to enhance adaption sensitivity, we find that in order to prevent overshoots from developing at the contact discontinuity, we require $p \geq 1.4$.

The Shu-Osher problem adds a one-dimensional idealization of smooth turbulent fluctuations to the sharp discontinuities considered above. Figure 9(a) presents density profiles of the Shu-Osher problem's shocklet-containing low-frequency oscillations as computed on a 192-point grid by the WENO-5 methods that appear in Fig. 8. Near the leftmost crest only the WENO-5/3 scheme with $p=1.4$ tracks the converged solution without minor oscillations. Density profiles of the smooth high-frequency fluctuations immediately upstream of the main shock are shown in Fig. 9(b). As we would expect, the increased adaption sensitivity of higher p values leads to unnecessary additional dissipation in "turbulent" regions; however, the WENO-5/3 scheme is marginally better able to resist this degradation than the WENO-5/5 scheme.

For the three-dimensional compressible turbulence configurations, we run all WENO-3 and WENO-4 methods with $p=1.0$ and all WENO-5 methods with $p=1.4$, and thus indications of p values will be suppressed. Figure 10 shows the temporal evolution in isotropic turbulence of turbulent kinetic energy for $N=64$ and initial $Re_\lambda=35$ and $M_t=0.7$ as computed by WENO-3/3, WENO-4/4, WENO-5/5, and WENO-5/3 schemes. Grid-converged results for $N=128$ are also included. Though the WENO-5 methods outperform the others, neither approaches grid convergence, and the profile generated by WENO-5/3 scheme does not differ discernibly from that of the WENO-5/5 scheme.

V. Quantified Computational Performance

In Table 4, we quantitatively summarize the increase in computational expense incurred and the reduction in numerical error achieved by each of the WENO schemes that we have presented in this paper. The simulations are of compressible isotropic turbulence for $N=64$, $Re_\lambda=35$, and $M_t=0.7$ and employ four processors in a 256-2.2 GHz Intel Xeon Prestonia cluster with a Myrinet interconnectivity switch for processor communication. Numerical error is defined as the decay of turbulent kinetic energy in excess of grid-converged results, for which $N=128$. Note that Figs. 5 and 10 compare the results of each WENO scheme to grid-converged results, and, alternatively, Table 4 compares the schemes only among themselves. The cost of implementing the relative smoothness-limiting procedure is negligible and may be completely disregarded. Newly apparent from this table is the observation that the WENO-4/4-RL scheme removes significantly

more numerical error than either WENO-5 method with only half as much increased computational time over the original WENO-3/3 scheme.

VI. Conclusions

We have described two distinct approaches to reducing the dissipation of WENO methods without compromising their shock-capturing capabilities for direct numerical simulations of compressible turbulence. Implementations of these modifications were tested in the inviscid shock tube and Shu-Osher problems, which are idealized one-dimensional cases, and decaying compressible isotropic turbulence, which is a canonical three-dimensional turbulent field.

Our results suggest that the technique of bandwidth-optimizing the WENO candidate stencils fails to meaningfully alter WENO performance. Although minor improvements are evident in the one-dimensional cases under the WENO-5/3 scheme versus the WENO-5/5 scheme, simulations of isotropic turbulent flow exhibit no differences that would favor the former. On the other hand, we find that the technique of constraining WENO adaption with a relative smoothness limiter both significantly enhances numerical accuracy for all tested problems and generates negligible additional computational expense. Also, the relative (as opposed to absolute) limiter appears to be broadly effective regardless of flow configuration when set to a value of one order of magnitude, which arises naturally from considerations of smooth waves. We therefore encourage the use of either the WENO-3/3-RL scheme or WENO-4/4-RL scheme for numerical simulations that employ WENO methods uniformly.

Acknowledgments

This work was sponsored by the National Science Foundation under Grant CTS-0238390 and the Air Force Office of Scientific Research under Grant AF/F49620-02-1-0361. Computational resources were provided by the CRoCCo Laboratory at Princeton University.

References

[1]Liu, X.-D., Osher, S., and Chan, T., "Weighted Essentially Non-Oscillatory Schemes," *Journal of Computational Physics*, Vol. 115, No. 1, 1994, pp. 200–12.

[2]Jiang, G.-S. and Shu, C.-W., "Efficient Implementation of Weighted ENO Schemes," *Journal of Computational Physics*, Vol. 126, No. 1, 1996, pp. 202–28.

[3]Garnier, E., Mossi, M., Sagaut, P., Comte, P., and Deville, M., "On the Use of Shock-Capturing Schemes for Large-Eddy Simulations," *Journal of Computational Physics*, Vol. 153, No. 1, 1999, pp. 273–311.

[4]Weirs, V. G., *A Numerical Method for the Direct Simulation of Compressible Turbulence*, Ph.D. thesis, University of Minnesota, December 1998.

[5]Martín, M. P., Taylor, E. M., Wu, M., and Weirs, V. G., "A Bandwidth-Optimized WENO Scheme for the Direct Numerical Simulation of Compressible Turbulence," Submitted to Journal of Computational Physics.

[6]Martín, M. P., "Shock-Capturing and the LES of High-Speed Flows," *Annual Research Briefs*, Center for Turbulence Research, 2000, pp. 193–8.

[7]Wu, M., Taylor, E. M., and Martín, M. P., "Assessment of STBLI DNS Data and Comparison Against Experiments," Paper 2005–4895, American Institute of Aeronautics and Astronautics, 2005.

[8]Lele, S. K., "Compact Finite-Difference Schemes with Spectral-Like Resolution," *Journal of Computational Physics*, Vol. 103, No. 1, 1992, pp. 16–42.

[9]Lockard, D. P., Brentner, K. S., and Atkins, H. L., "High-Accuracy Algorithms for Computational Aeroacoustics," *AIAA Journal*, Vol. 33, No. 2, 1995, pp. 246–51.

[10]Ponziani, D., Pirozzoli, S., and Grasso, F., "Development of Optimized Weighted-ENO Schemes for Multiscale Compressible Flows," *International Journal for Numerical Methods in Fluids*, Vol. 42, No. 9, 2003, pp. 953–77.

WENO-3/3		
Stencil	$\varepsilon = 1.1\%$	$\varepsilon = 2.5\%$
Optimal	0.497	0.525
$k = 0$	0.142	0.176
$k = 1$	0.246	0.304
$k = 2$	0.246	0.304
$k = 3$	0.142	0.176

Table 1. Bandwidth-resolving efficiency indices for the optimal and candidate stencils of the 3-point/3rd-order symmetric WENO scheme.

$\varepsilon = 1.0\%$			
Stencil	WENO-5/5	WENO-5/3	Improvement
Optimal	0.628	0.646	+3%
$k = 0$	0.186	0.159	−15%
$k = 1$	0.263	0.364	+38%
$k = 2$	0.350	0.408	+17%
$k = 3$	0.350	0.408	+17%
$k = 4$	0.263	0.364	+38%
$k = 5$	0.186	0.159	−15%

Table 2. Comparison of the bandwidth-resolving efficiency indices for the optimal and candidate stencils of 5-point/5th-order and 5-point/3rd-order symmetric WENO schemes. Error tolerance $\varepsilon = 1.0\%$.

$\varepsilon = 2.5\%$			
Stencil	WENO-5/5	WENO-5/3	Improvement
Optimal	0.654	0.670	+2%
$k = 0$	0.222	0.444	+100%
$k = 1$	0.314	0.398	+27%
$k = 2$	0.414	0.459	+11%
$k = 3$	0.414	0.456	+11%
$k = 4$	0.314	0.399	+27%
$k = 5$	0.222	0.445	+100%

Table 3. Comparison of the bandwidth-resolving efficiencies for the optimal and candidate stencils of 5-point/5th-order and 5-point/3rd-order symmetric WENO schemes. Error tolerance $\varepsilon = 2.5\%$.

Scheme	Run Time Relative to WENO-3/3	Error Relative to WENO-3/3	Error Relative to WENO-3/3-RL
WENO-3/3	0%	0%	+160%
WENO-3/3-RL		−62%	0%
WENO-4/4	+26%	−63%	−3%
WENO-4/4-RL		−93%	−83%
WENO-5/5	+56%	−72%	−28%
WENO-5/3		−73%	−29%

Table 4. Relative performance characteristics in isotropic turbulence of various symmetric WENO schemes, including schemes employing the relative smoothness limiter (RL) and the scheme employing bandwidth-optimized candidate stencils (WENO-5/3). The error is defined as excess decay of turbulent kinetic energy.

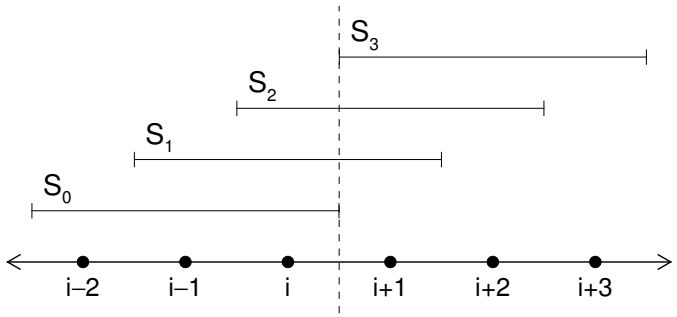

Figure 1. Symmetric WENO candidate stencils for approximating the numerical flux $\hat{f}^{+}_{i+1/2}$ when the number of points per candidate stencil is $r = 3$.

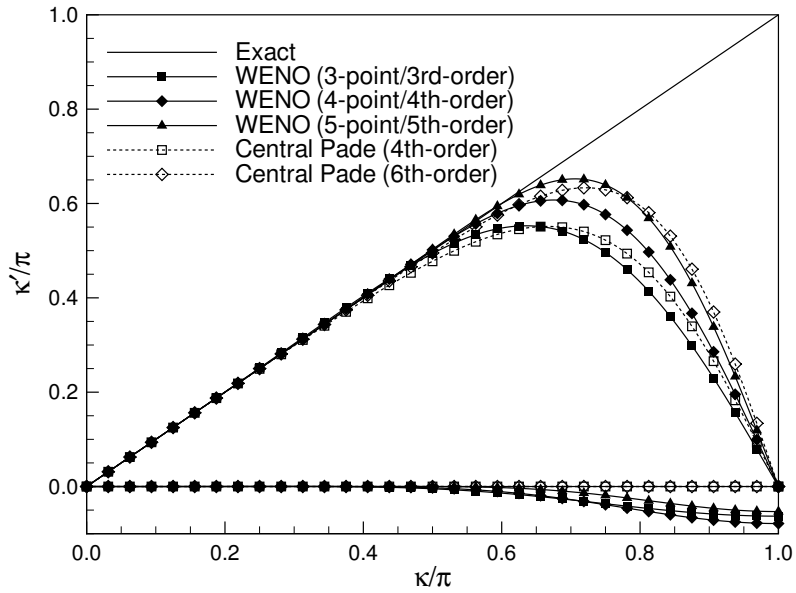

Figure 2. Bandwidth properties of the bandwidth-optimized optimal stencils of various symmetric WENO schemes and, for reference, well-established central Padé schemes. Positive κ' indicates phase and negative κ' indicates amplitude.

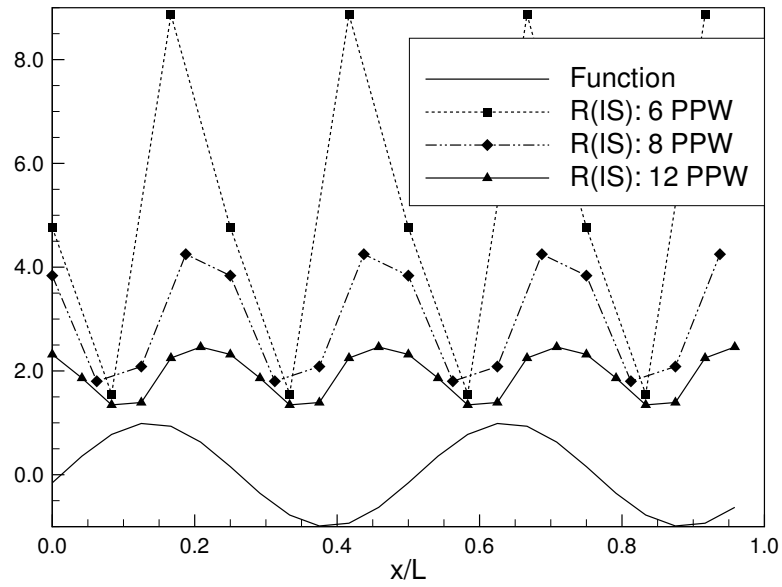

Figure 3. Ratio of the maximum to minimum WENO smoothness measurement IS_k for a smooth sinusoidal function on grids providing varying points per wavelength (PPW).

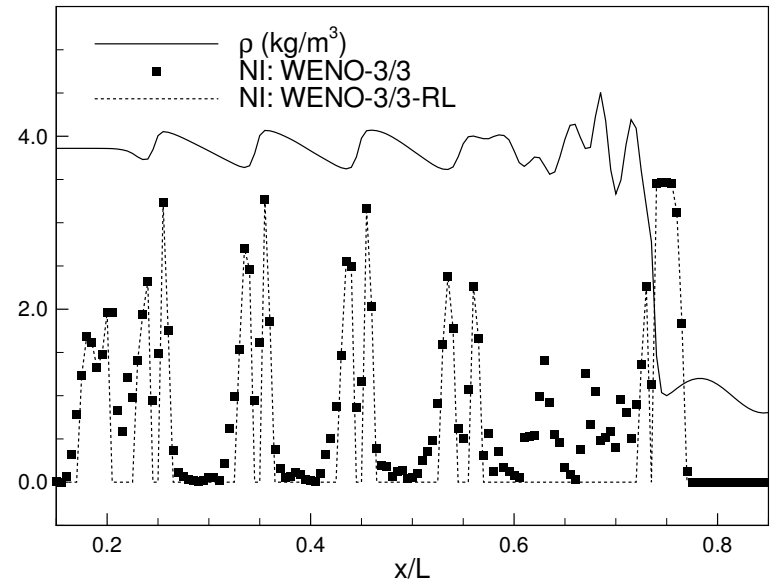

(a) Profiles of nonlinearity index.

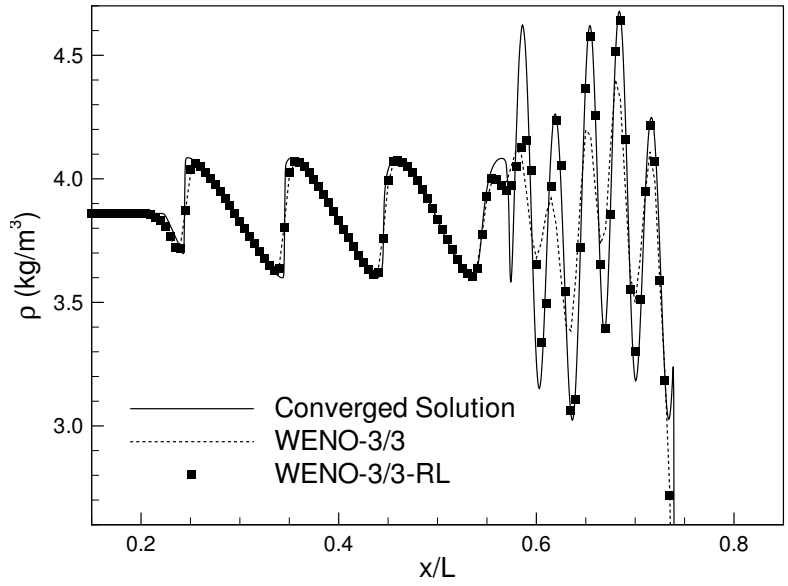

(b) Density profiles.

Figure 4. Comparison of 3-point/3rd-order symmetric WENO schemes with and without a relative smoothness limiter (RL) for simulations of the Shu-Osher problem.

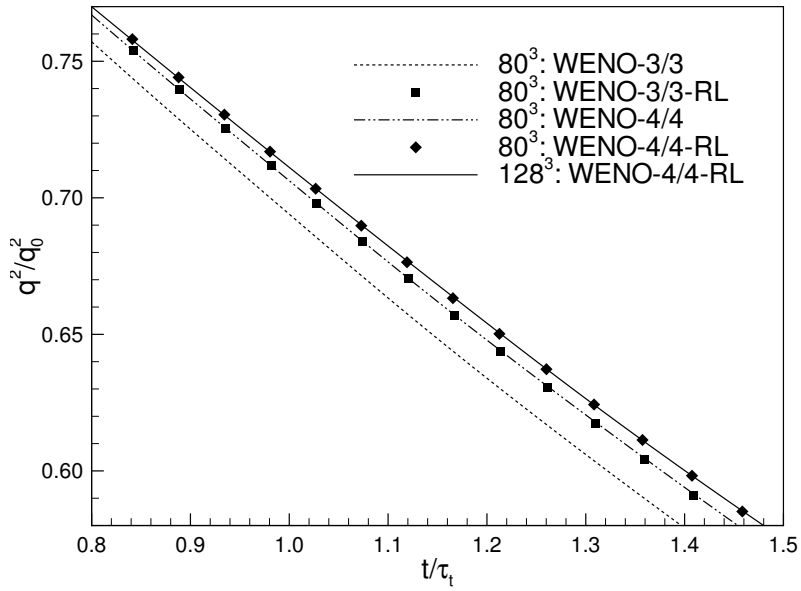

Figure 5. Temporal evolution of the average turbulent kinetic energy q^2 (normalized by its initial value) in compressible isotropic turbulence for symmetric WENO schemes with and without a relative smoothness limiter (RL).

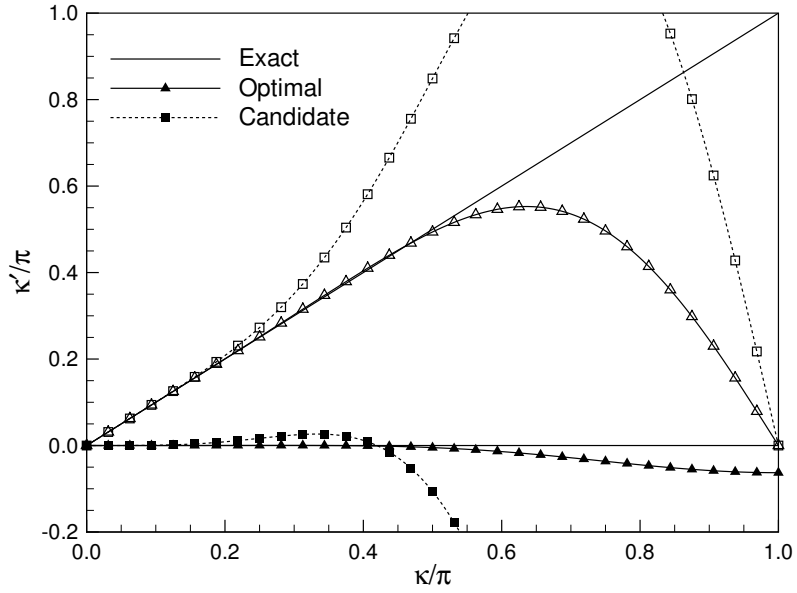

(a) Stencil $k = 0$.

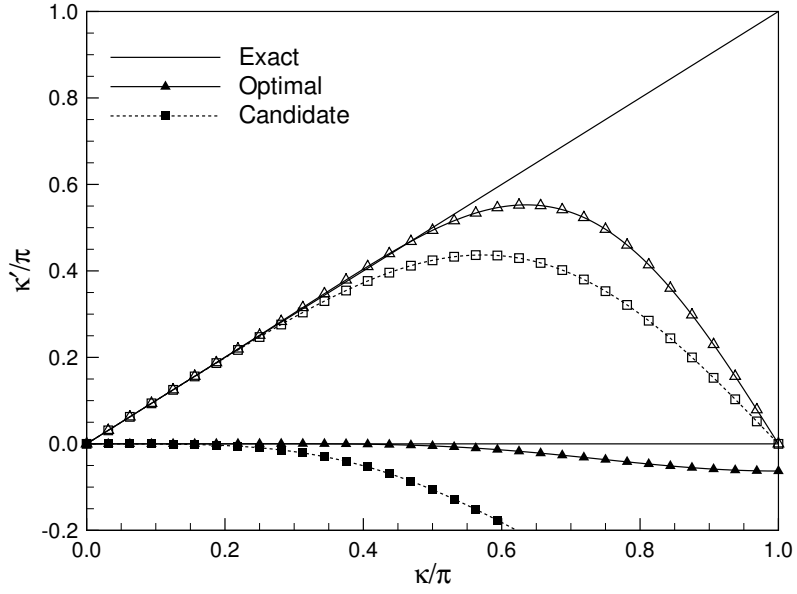

(b) Stencil $k = 1$.

Figure 6. Bandwidth properties of selected order-optimized 3-point WENO candidate stencils and, for reference, the WENO-3/3 optimal stencil. Open and filled symbols indicate phase and amplitude, respectively.

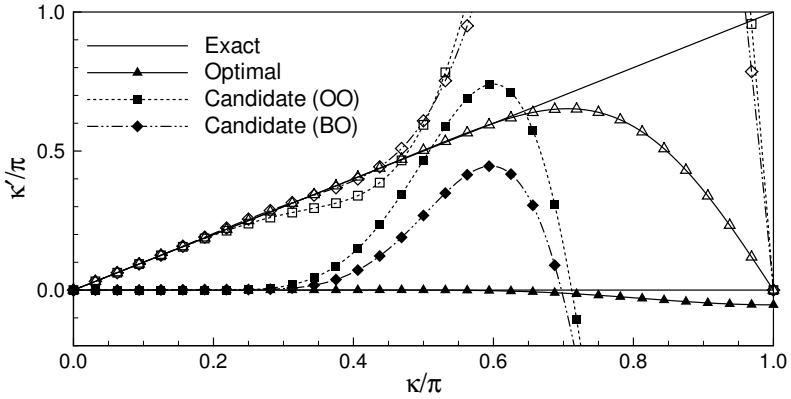

(a) Stencil $k = 0$.

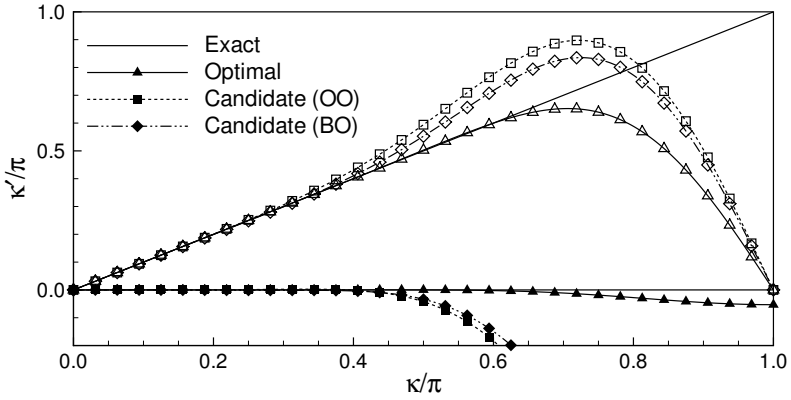

(b) Stencil $k = 1$.

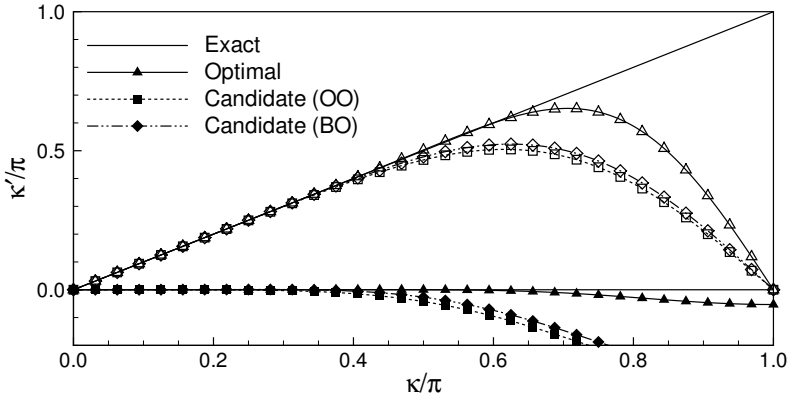

(c) Stencil $k = 2$.

Figure 7. Bandwidth properties of selected 5-point WENO candidate stencils under both order optimization (5th-order) and bandwidth optimization (3rd-order) and, for reference, the WENO-5/5 optimal stencil. Open and filled symbols indicate phase and amplitude, respectively.

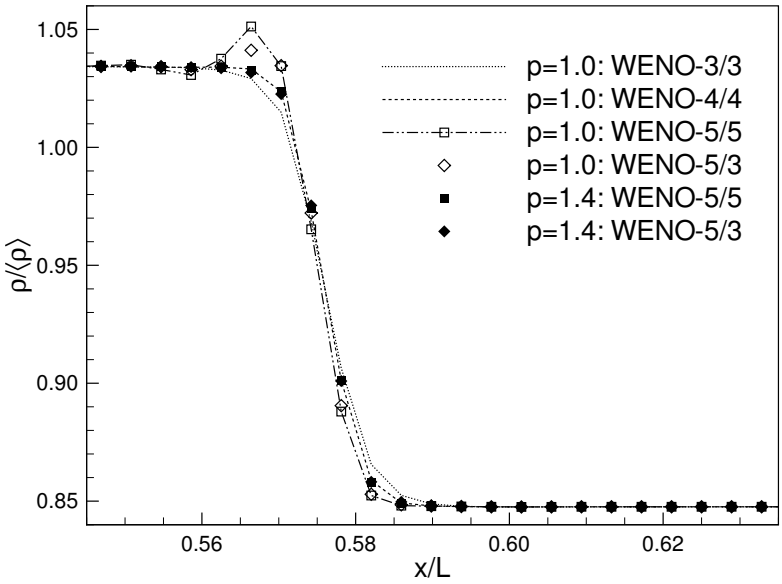

Figure 8. Density profiles across the contact discontinuity in an inviscid shock tube for symmetric WENO schemes *not* employing a smoothness limiter.

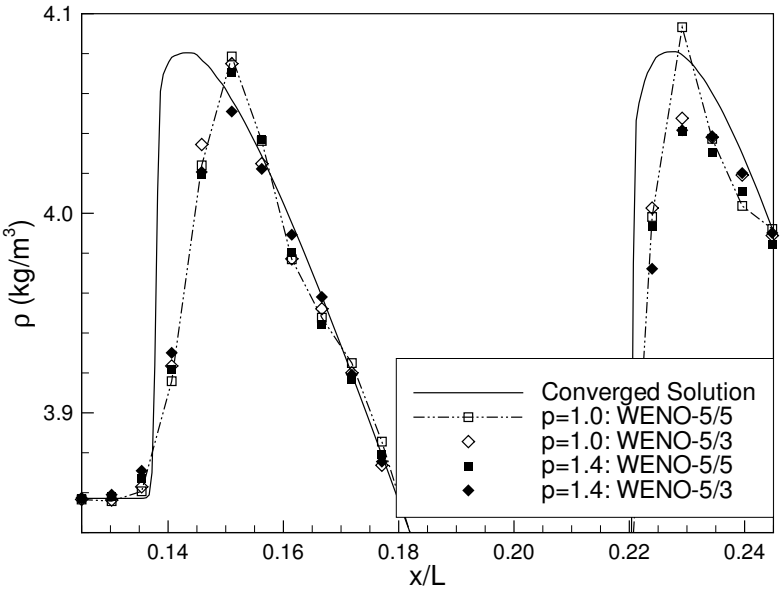

(a) Low-frequency region (with shocklets).

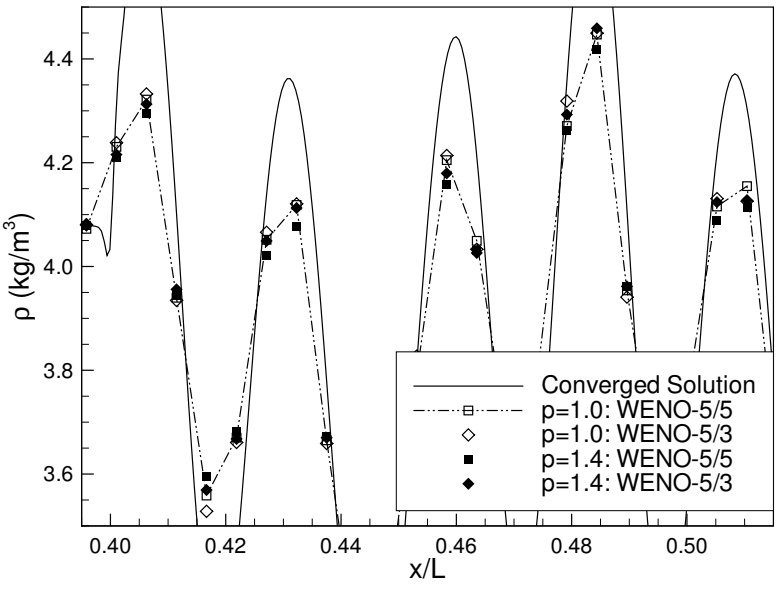

(b) High-frequency region.

Figure 9. Density profiles downstream of the main shock for the Shu-Osher problem with symmetric WENO schemes *not* employing a smoothness limiter.

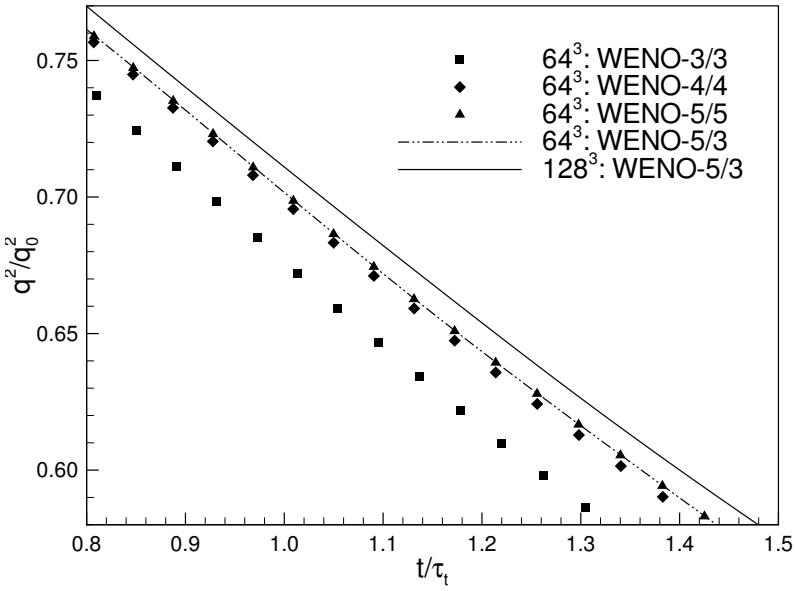

Figure 10. Temporal evolution of the average turbulent kinetic energy q^2 (normalized by its initial value) in compressible isotropic turbulence for symmetric WENO schemes *not* employing a smoothness limiter.